The Durham/UKST Galaxy Redshift Survey - II. The Field Galaxy Luminosity Function.

A. Ratcliffe[1], T. Shanks[1], Q.A. Parker[2] and R. Fong[1]

[1] *Physics Deptartment, University of Durham, South Road, Durham, DH1 3LE.*
[2] *Anglo-Australian Observatory, Coonabarabran, NSW 2357, Australia.*

1 February 2008

ABSTRACT
We present the results for the galaxy luminosity function as estimated from the Durham/UKST Galaxy Redshift Survey. This survey is magnitude limited to $b_J \sim 17$, contains ~ 2500 galaxies sampled at a rate of one in three and surveys a $\sim 4 \times 10^6 (h^{-1}\mathrm{Mpc})^3$ volume of space. The maximum likelihood parameters for a standard Schechter luminosity function are estimated to be $M^*_{b_J} = -19.72 \pm 0.09$, $\alpha = -1.14 \pm 0.08$ and $\phi^* = (1.2 \pm 0.2) \times 10^{-2}$ $(h^3\mathrm{Mpc}^{-3})$. Attempting to correct for the scatter in the observed magnitudes leads to a flatter faint end slope, $\alpha = -1.04 \pm 0.08$, which, combined with the different luminosity function shape, causes a higher normalisation to be estimated, $\phi^* = (1.7 \pm 0.3) \times 10^{-2}$ $(h^3\mathrm{Mpc}^{-3})$. Neither of these parametric functions provides a good formal fit to the non-parametric estimate of the luminosity function. A comparison with galaxy luminosity functions from other redshift surveys shows good agreement and the shape of the luminosity function now appears well-defined down to $M_{b_J} \simeq -17$. There are some discrepancies between the different surveys for galaxies fainter than this absolute magnitude. However, our estimate agrees well with that from the APM-Stromlo Galaxy Redshift Survey and we measure a fairly flat faint end slope.

Key words: galaxies: luminosity function – galaxies: general – cosmology: observations – large-scale structure of Universe.

1 INTRODUCTION

The galaxy luminosity function is a fundamental quantity in observational cosmology. Indeed, a knowledge of its form it is essential for an accurate analysis of galaxy clustering in magnitude limited redshift surveys (e.g. Efstathiou 1988) and also for a proper interpretation of the observed galaxy number-magnitude counts (e.g. Metcalfe et al. 1995a). On the theoretical side, the luminosity function is one of the first tests that models of galaxy formation and evolution must pass in order to be called successful (e.g. Cole et al. 1994).

Current interest in the observed galaxy luminosity function takes the form of an accurate determination of the faint end slope and overall normalisation (e.g. Marzke et al. 1994; Vettolani et al. 1996), the relationship between the field and cluster luminosity functions (e.g. Driver et al. 1994; Kashikawa et al. 1995) and the evolution with redshift of the luminosity function (Lilly et al. 1995; Ellis et al. 1996). Meanwhile, theoreticians are attempting to improve the sophistication of their modelling in order to predict more realistic luminosity functions (e.g. Frenk et al. 1996).

The initial clustering results, redshift maps, etc. of the

Durham/UKST Galaxy Redshift Survey were summarized in the first paper of this series (Ratcliffe et al. 1996). In this paper we present a detailed analysis of the luminosity function and space density of galaxies in this optically selected survey. We briefly describe our survey in Section 2. The techniques used to estimate the luminosity function, radial density and normalisation are outlined in Section 3. The results from the Durham/UKST survey are then presented in Section 4. Section 5 compares and discusses the current state of the galaxy luminosity function. Finally, in Section 6 we summarize our conclusions from this analysis.

2 THE DURHAM/UKST GALAXY REDSHIFT SURVEY

The Durham/UKST Galaxy Redshift Survey was constructed using the FLAIR fibre optic system (Parker & Watson 1995) on the 1.2m UK Schmidt Telescope at Siding Spring, Australia. This survey is based on the astrometry and photometry from the Edinburgh/Durham Southern Galaxy Catalogue (EDSGC; Collins, Heydon-Dumbleton & MacGillivray 1988; Collins, Nichol & Lumsden 1992) and

was completed in 1995 after a 3-yr observing programme. The survey itself covers a $\sim 20° \times 75°$ area centered on the South Galactic Pole (60 UKST plates) and is sparse sampled at a rate of one in three of the galaxies to $b_J \simeq 17$ mag. The resulting survey contains ~ 2500 redshifts, probes to a depth greater than $300h^{-1}$Mpc, with a median depth of $\sim 150h^{-1}$Mpc, and surveys a volume of space $\sim 4 \times 10^6 (h^{-1}\mathrm{Mpc})^3$.

The survey is >75 per cent complete to the nominal magnitude limit of $b_J = 17.0$ mag. This incompleteness was mainly caused by poor observing conditions, intrinsically low throughput fibres and other various observational effects. In a comparison with ~ 150 published galaxy velocities (Peterson et al. 1986; Fairall & Jones 1988; Metcalfe et al. 1989; da Costa et al. 1991) our measured redshifts had negligible offset and were accurate to $\pm 150\,\mathrm{kms}^{-1}$. The scatter in the EDSGC magnitudes has been estimated at ± 0.22 mags (Metcalfe, Fong & Shanks 1995b) for a sample of ~ 100 galaxies. This scatter has been confirmed by a preliminary analysis of a larger sample of high quality CCD photometry. All of these observational details are discussed further in a forthcoming data paper (Ratcliffe et al., in preparation).

3 ESTIMATING THE LUMINOSITY FUNCTION, RADIAL DENSITY AND NORMALISATION

We have estimated the galaxy luminosity function, $\phi(L)$, from the Durham/UKST Galaxy Redshift Survey firstly using the very basic and common method of Schmidt (1968) and secondly using two maximum likelihood techniques; the parametric method proposed by Sandage, Tammann & Yahil (1979) and the non-parametric stepwise maximum likelihood method of Efstathiou, Ellis & Peterson (1988). These methods have well defined error properties and the maximum likelihood techniques have been constructed such that they are unbiased by density inhomogeneities in the galaxy distribution. They assume that the luminosity function has a universal form and hence the number density is separable into a product of functions of luminosity and position, $n(L,\mathbf{r}) = \phi(L)\rho(\mathbf{r})$. Unfortunately, in using this assumption all the density and normalisation information is lost. To obtain the radial density information one uses a similar technique to the above non-parametric method as proposed by Saunders et al. (1990). To determine the absolute normalisation the minimum variance iterative technique of Loveday et al. (1992) is employed. This is a development of the method originally proposed by Davis & Huchra (1982).

3.1 The Luminosity Function

Probably the most basic estimator of the luminosity function is the '$1/V_{max}$' method due to Schmidt (1968)

$$\phi(L)dL = \sum_i \frac{1}{V_{max}(L_i)}, \tag{1}$$

where the sum extends over all galaxies in the $L \to L + dL$ luminosity interval and $V_{max}(L_i)$ is the maximum volume that the galaxy of luminosity L_i could be seen in (given the survey's physical and apparent magnitude limits). Unfortunately, this estimate is biased by density inhomogeneities in

the galaxy distribution but is still useful for initial comparisons. Error properties of this method can be estimated by a simple rms of the galaxies in each luminosity interval in question

$$\mathrm{Var}(\phi) = \sum_i \frac{1}{V_{max}^2(L_i)}, \tag{2}$$

For future reference this will be called the VMAX method.

Methods that are independent of the galaxy density inhomogeneities can be constructed as follows. One can form a likelihood, $\mathcal{L}$, based on the probability of observing a galaxy of luminosity L_i at redshift z_i in a magnitude limited redshift survey

$$p_i \propto \phi(L_i) \left/ \int_{L_{min}(z_i)}^{\infty} \phi(L)dL \right. , \tag{3}$$

where

$$\mathcal{L} = \prod_{i=1}^{N} p_i. \tag{4}$$

The product extends over all of the N galaxies in the survey and $L_{min}(z_i)$ is the minimum absolute luminosity that a galaxy at redshift z_i could have and still be included in the survey. A maximum absolute luminosity could also be incorporated into equation 3, altering the upper limit of the integral. In practice this makes little difference to any results. The best estimate of $\phi(L)$ is then given when $\mathcal{L}$ (or equivalently $\ln \mathcal{L}$) is maximised.

In the parametric case one assumes a function form for $\phi(L)$ and maximises equation 4 with respect to the parameters of this assumed functional form (Sandage et al. 1979). In keeping with tradition we use the 'Schechter function' (Schechter 1976) to describe $\phi(L)$

$$\phi(L)dL = \phi^* \left(\frac{L}{L^*}\right)^\alpha \exp\left(-\frac{L}{L^*}\right) d\left(\frac{L}{L^*}\right), \tag{5}$$

where the three parameters are a normalisation, ϕ^*, a faint end slope, α, and a characteristic luminosity, L^*, (or equivalently absolute magnitude, M^*). In practice ϕ^* cancels from equation 3 and a maximum is determined in the (M^*, α) likelihood space. A further consideration is the effect of the observed scatter in the measured magnitudes. Efstathiou et al. (1988) modelled this by approximating these errors with a Gaussian distribution of zero mean and σ rms. The observed (convolved) Schechter function, ϕ_o, then becomes

$$\phi_o(M) = \frac{1}{\sqrt{2\pi}\sigma} \int_{-\infty}^{\infty} \phi(M') \exp\left[-\frac{1}{2\sigma^2}(M'-M)^2\right] dM', \tag{6}$$

Given that equation 6 is a slightly naive approximation it is not obvious that it will substantially improve the quality of the fit. Finally, error properties of this method can be estimated by the deviations of $\mathcal{L}$ from its maximum value. One can plot error ellipses in the (M^*, α) plane by considering the contours corresponding to

$$\ln \mathcal{L} = \ln \mathcal{L}_{max} - \frac{1}{2}\chi_\beta^2(n), \tag{7}$$

where $\mathcal{L}_{max}$ is the maximum likelihood, n is the number of free parameters (namely two, α and M^*) and β is the required confidence level for that number of free parameters. For future reference this will be called the STY method.

In the non-parametric case one assumes that $\phi(M)$ can be written as a series of constant steps across given luminosity intervals and one maximises to find the relative values of these steps (Efstathiou et al. 1988)

$$\phi(M) = \phi_k, \quad |M - M_k| \le \Delta M/2, \quad k = 1, \ldots, N_p, \qquad (8)$$

where N_p is the number of constant steps (or bins) of width ΔM. The maximisation condition ($\frac{\partial \ln \mathcal{L}}{\partial \phi_k} = 0$) quickly leads to an equation that can be solved iteratively

$$\phi_k = \frac{\sum_{i=1}^{N} W(M_i - M_k)}{\sum_{i=1}^{N} \left[\frac{H(M_k - M_{min}(z_i))\Delta M}{\sum_{j=1}^{N_p} H(M_j - M_{min}(z_i))\phi_j \Delta M} \right]}, \qquad (9)$$

where

$$W(x) = \begin{cases} 1 & |x| \le \Delta M/2 \\ 0 & \text{otherwise} \end{cases}, \qquad (10)$$

and

$$H(x) = \begin{cases} 0 & x \le -\Delta M/2 \\ \frac{1}{2} + \frac{x}{\Delta M} & |x| \le \Delta M/2 \\ 1 & x \ge \Delta M/2 \end{cases}. \qquad (11)$$

Finally, error properties of the ϕ_k's can be estimated from the covariance matrix

$$\text{Cov}(\phi_k) = -\left(\frac{\partial^2 \ln \mathcal{L}}{\partial \phi_l^2} \right)^{-1}_{\phi_l = \phi_k}. \qquad (12)$$

A constraint involving the ϕ_k's is usually introduced into the likelihood equation in order to ensure that the information matrix is non-singular and hence invertible as is assumed in equation 12. This constraint does not affect the shape of the maximum likelihood solution. We take a simple approach and fix one of the maximum likelihood ϕ_k's to be constant. We then assume that one can neglect the off-diagonal elements (Saunders et al. 1990). Using this assumption gives

$$\begin{aligned} \text{Var}(\phi_k) = & \left(\sum_{i=1}^{N} \left[\frac{W(M_i - M_k)}{\phi_k^2} \right] \right. \\ & \left. - \sum_{i=1}^{N} \left[\frac{H(M_k - M_{min}(z_i))\Delta M}{\sum_{j=1}^{N_p} H(M_j - M_{min}(z_i))\phi_j \Delta M} \right]^2 \right)^{-1}. \end{aligned}$$

In practice the cross-derivatives are small and therefore our approximation will only slightly underestimate the errors in the ϕ_k. For future reference this will be called the SWML method.

A major problem with the STY method is that it will always return a maximum likelihood solution regardless of the assumed parametric form and how well it represents the actual luminosity function. Therefore, it is necessary to test the goodness of fit of this solution with a likelihood ratio test. We assume that the non-parametric SWML method provides a good representation of the actual luminosity function shape. Let $\mathcal{L}_1$ be the likelihood calculated using the maximum likelihood solution of the given parametric form (STY) and let $\mathcal{L}_2$ be the likelihood calculated using the maximum likelihood solution of the ϕ_k's (SWML). Efstathiou et al. (1988) have shown that $2\ln(\mathcal{L}_1/\mathcal{L}_2)$ approximately behaves like a χ^2 statistic with $(N_p - 3)$ degrees of freedom. However, for the answer to be independent of the bin size

and the number of bins, the likelihood $\mathcal{L}_1$ should be calculated using the SWML likelihood formula (which produced $\mathcal{L}_2$) with the set of ϕ_k's from

$$\phi_k \simeq \frac{\int \phi(L)dN(L)}{\int dN(L)} \simeq \frac{\int \phi(L)L^{\frac{3}{2}} dL}{\int L^{\frac{3}{2}} dL}. \qquad (13)$$

The integrals in equation 13 are over the luminosity interval in question, $[L_k - \frac{\Delta L}{2}, L_k + \frac{\Delta L}{2}]$ (Efstathiou et al. 1988; Saunders et al. 1990).

3.2 The Radial Density

Using a similar method to Section 3.1 one can estimate the radial density function, $\rho(r)$. First consider the probability of observing a galaxy of luminosity L_i at redshift z_i in a magnitude limited redshift survey. As before a likelihood is formed from the product of these probabilities

$$\mathcal{L} = \prod_{i=1}^{N} \frac{\rho(z_i)}{\int_{\max[z_{low}, z_{min}(L_i)]}^{\min[z_{hi}, z_{max}(L_i)]} \rho(z_i) \left(\frac{dV}{dz}\right) dz}, \qquad (14)$$

where $z_{min}(L_i)$ and $z_{max}(L_i)$ are the minimum and maximum redshifts at which a galaxy of luminosity L_i could be seen and still be included in the survey. Saunders et al. (1990) assume that one can write $\rho(r)$ as a series of step functions in radial distance and then solve for the maximum likelihood ρ_k's by iteration as before. Finally, error properties of the ρ_k's can be estimated from the appropriate covariance matrix and we use similar approximations to those made in Section 3.1 to simplify the analysis involved.

3.3 The Normalisation

By their method of construction these maximum likelihood techniques cannot provide an overall normalisation. Therefore, one must adopt other techniques to estimate the mean space density of galaxies, $\bar{n}$, and the normalisation of the luminosity function, ϕ^*.

The expected distribution of the number of galaxies as a function of distance r is given by

$$n(r) = f\bar{n} \, V(r) \, S(r), \qquad (15)$$

where f is the sampling rate of the survey, $\bar{n}$ is the mean spatial galaxy density of the survey and $V(r)$ is the volume element of the survey at a distance r. The radial selection function of the survey, $S(r)$, is given by

$$S(r) = \frac{\int_{\max[L_{low}, L_{min}(r)]}^{\infty} \phi(L)dL}{\int_{L_{low}}^{\infty} \phi(L)dL}, \qquad (16)$$

where L_{low} is some minimum absolute galaxy luminosity and $L_{min}(r)$ was defined in Section 3.1. If a Schechter function is assumed then the above integrals become incomplete Gamma functions, $\Gamma(\alpha + 1, x)$. The mean spatial galaxy density is also related to the luminosity function by

$$\bar{n} = \int_{L_{low}}^{\infty} \phi(L)dL, \qquad (17)$$

and so using the luminosity function from either equation 5 or 6 one finds a relationship involving $\bar{n}$, ϕ^* and an integral over the shape of the assumed functional form. Using this

formalism Davis & Huchra (1982) showed that an unbiased estimator for $\bar{n}$ is given by

$$\bar{n} = \frac{\sum_{i=1}^{N} w(r_i)/f}{\int_{r_{min}}^{r_{max}} S(r)w(r)dV}, \qquad (18)$$

where $w(r)$ is any weight function we choose and $[r_{min}, r_{max}]$ is the distance range over which we use galaxies. One choice is to weight all galaxies equally, whereby $w = 1$. However, Davis & Huchra (1982) showed that the minimum variance in $\bar{n}$ occurs when

$$w(r) = \frac{1}{1 + 4\pi f\bar{n}J_3(r_c)S(r)}, \qquad (19)$$

where

$$J_3(r_c) = \int_0^{r_c} x^2 \xi(x)dx, \qquad (20)$$

r_c is the scale on which J_3 converges to a maximum value and $\xi(x)$ is the galaxy 2-point correlation function. Given that this weighting depends on the quantity we are interested in ($\bar{n}$), Loveday et al. (1992) have developed an iterative scheme involving equations 18 and 19. This method should produce the minimum variance estimate of $\bar{n}$ if $J_3(r_c)$ converges on a scale r_c smaller than the survey. The variance of $\bar{n}$ is given by (Davis & Huchra 1982)

$$\mathrm{Var}(\bar{n}) = \frac{\bar{n}\int w^2 S dV + f\bar{n}^2 \int w_1 w_2 S_1 S_2 \xi(x_{12})dV_1 dV_2}{f\left(\int w S dV\right)^2}. \qquad (21)$$

In practice the final answer for $\bar{n}$ (and hence ϕ^*) depends little on the value of $J_3(r_c)$ used. Therefore, we adopt the value $4\pi J_3(r_c) = 5000h^{-3}\mathrm{Mpc}^3$ and doubling or halving this only makes a few per cent difference to $\bar{n}$. Also, we are free to choose the value of L_{low} (or equivalently M_{low}) in equations 16 and 17 as long as we are consistent and throw away all the fainter galaxies from the sum in the numerator of equation 18. Obviously $\bar{n}$ is very sensitive to the value of M_{low} used but ϕ^* is very stable over a range of ~ 5 magnitudes.

4   RESULTS FROM THE DURHAM/UKST GALAXY REDSHIFT SURVEY

We use galaxies in the distance range $[5,350]h^{-1}\mathrm{Mpc}$, where the minimum distance comes from requiring a reliable redshift distance estimate (relatively unaffected by peculiar velocities) and the maximum distance is due to the magnitude limits of the survey. We assume a $q_0 = \frac{1}{2}$, $\Lambda = 0$ cosmology and so comoving distances are given by

$$r(z) = \left(\frac{2c}{H_0}\right)\left[1 - \frac{1}{\sqrt{1+z}}\right], \qquad (22)$$

where $H_0 = 100h$ kms^{-1}Mpc^{-1} is the Hubble constant and c is the velocity of light in kms^{-1}. Volumes are calculated from the comoving distances and use

$$V = \frac{d\Omega}{3}r^3(z), \qquad (23)$$

where $d\Omega$ is the solid steradian angle of the survey. Absolute (M) and apparent (m) magnitudes are related by

$$5\lg d_L(z) = m - M - 25 - k_{corr}(z), \qquad (24)$$

Table 1. STY maximum likelihood results and normalisations assuming the pure Schechter function of equation 5, ϕ, and the convolved Schechter function of equation 6, ϕ_o.

	ϕ	ϕ_o
α	-1.14 ± 0.08	-1.04 ± 0.08
$M_{b_J}^*$ $(h=1)$	-19.72 ± 0.09	-19.68 ± 0.10
Prob.	0.16	0.22
$\bar{n}$ $(h^3\mathrm{Mpc}^{-3})$	$(6.4 \pm 1.1) \times 10^{-2}$	$(4.4 \pm 0.8) \times 10^{-2}$
ϕ^* $(h^3\mathrm{Mpc}^{-3})$	$(1.2 \pm 0.2) \times 10^{-2}$	$(1.7 \pm 0.3) \times 10^{-2}$

where

$$d_L(z) = (1+z)\,r(z), \qquad (25)$$

is the luminosity distance in h^{-1}Mpc and k_{corr} is the k-correction. A simple k-correction is used for all galaxies independent of morphological type

$$k_{corr} = k_1 z + k_2 z^2, \qquad (26)$$

where $k_1 = +3.15$ and $k_2 = -0.29$ (Broadbent 1994). Given the redshift range of interest this k-correction is more than adequate for this analysis.

The survey's magnitude limits were chosen by the authors to maximize depth and minimize observational incompleteness. In this case each of the 60 UKST fields has a different magnitude limit and our best sample contains 2055 redshifts with $\langle m_{lim}\rangle = 16.86 \pm 0.25$ mags and an average completeness of 75 per cent. Selection effects like this have been shown to cause no systematic biases in our methods of analysis (Ratcliffe 1996). One can check the completeness of this sample by using Schmidt's (1968) $\langle V/V_{max}\rangle$ test. For a uniform distribution of galaxies in a complete magnitude limited sample $\langle V/V_{max}\rangle = 0.5$, with a rms dispersion of $1/\sqrt{12N}$ (in the absence of clustering). If $\langle V/V_{max}\rangle$ is significantly lower or higher than 0.5 then we are missing objects at high or low redshift, respectively. For the above best sample we find that $\langle V/V_{max}\rangle = 0.50 \pm 0.01$ and so we are not systematically missing galaxies at any redshift.

4.1   The Luminosity Function Shape

Using the magnitude limits from the previous section the STY parametric solution has been calculated from the Durham/UKST survey for a pure Schechter function (equation 5) and a convolved Schechter function (equation 6). Following Metcalfe et al. (1995b) we use $\sigma = 0.22$ in equation 6 for the rms scatter in the observed magnitudes. Small variations in this parameter do not significantly affect the final results. The maximum likelihood results for α and M^* are shown in Table 1 and assume $h = 1$. The SWML nonparametric solution has similarly been calculated from the Durham/UKST survey, taking ~ 20 iterations for 5 *s.f.* convergence. These maximum likelihood solutions are all shown in Fig. 1, along with the basic VMAX estimate of the luminosity function, where we have scaled the ϕ's to agree in the bin containing the most galaxies ($M_{b_J} = -19.75$). We are only considering the shape of the luminosity function here and so the absolute normalisation is still arbitrary. The inset of Fig. 1 shows the joint 68 per cent error ellipsoids for the two STY solutions as calculated from equation 7, while
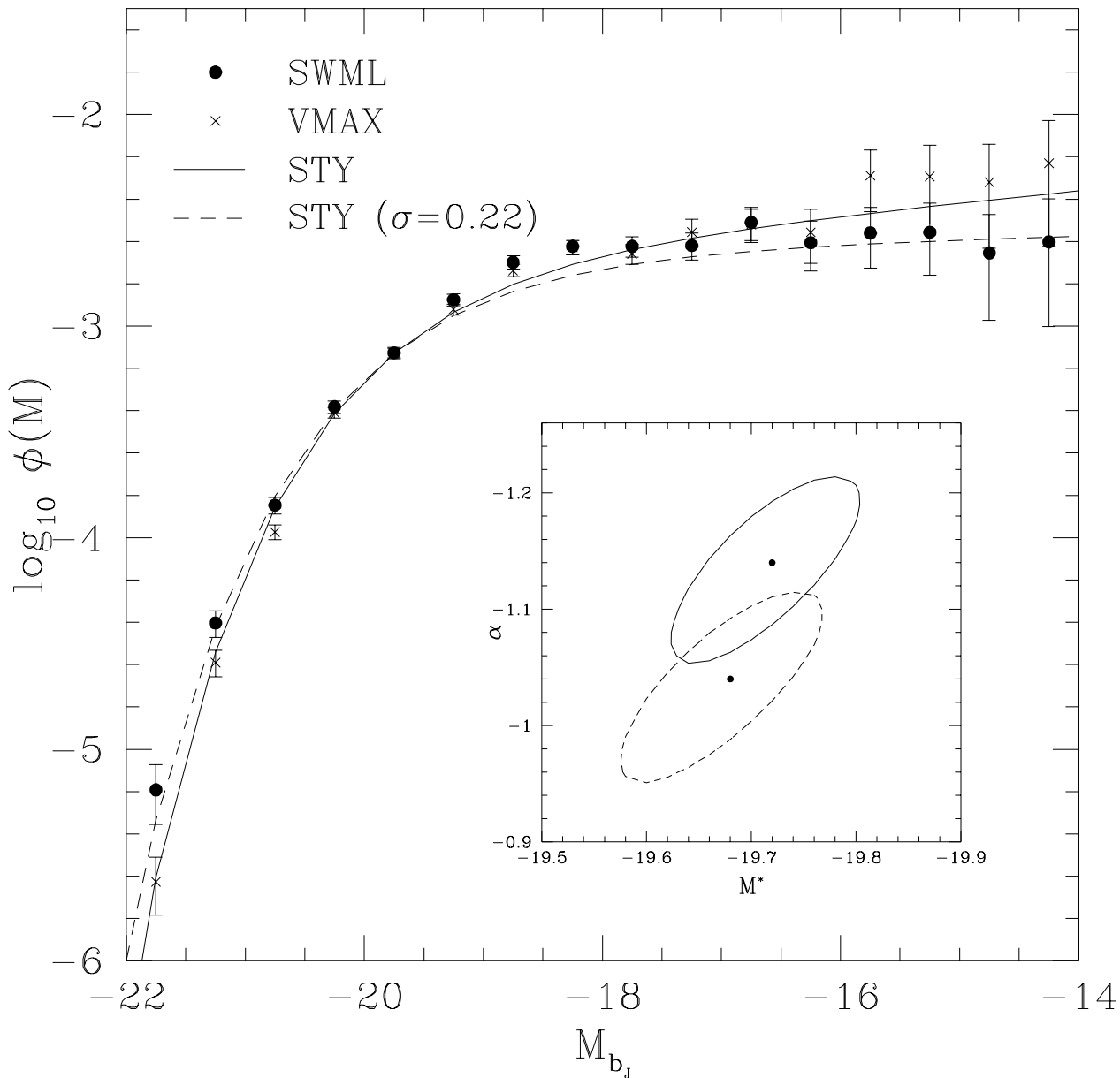
Figure 1. The galaxy luminosity function maximum likelihood solutions for a stepwise function (dots), a pure Schechter function (solid curve) and a convolved Schechter function (dashed curve). Also shown for comparison is the basic VMAX luminosity function estimate (crosses). These four solutions are scaled to agree at $M_{b_J} = -19.75$ but the overall normalisation is arbitrary at this stage. The inset shows the STY maximum likelihood results and joint 68 per cent error ellipsoids on both parameters in the (M^*, α) plane.

the errors quoted in Table 1 are the 1σ error on an individual parameter. The VMAX and SWML error bars on Fig. 1 were calculated from equations 2 and 13, respectively.

The observational incompleteness described in Section 2 is not explicitly accounted for in the luminosity function shape analysis presented here. To get around this problem one can weight the p_i's of equation 3 by the appropriate completeness rate depending on the UKST field and apparent magnitude interval in question. In practice, this correction made very little or no difference to the either the STY or the SWML maximum likelihood solutions.

A comparison of the two STY solutions in Fig. 1 shows that the main effect of the magnitude errors on a luminosity function of this shape is to pull $\phi(M)$ down at faint magnitudes while pushing it up slightly at bright magnitudes, essentially flattening it overall. The VMAX and SWML estimates both agree well except at the very bright and very faint ends. Such a faint end excess is expected if there local overdensity, see Fig. 2, and rejecting all galaxies within $r < 20h^{-1}$Mpc brings the VMAX estimate into line with the SWML one. The STY and SWML estimates both have relatively flat faint end slopes with no convincing evidence for
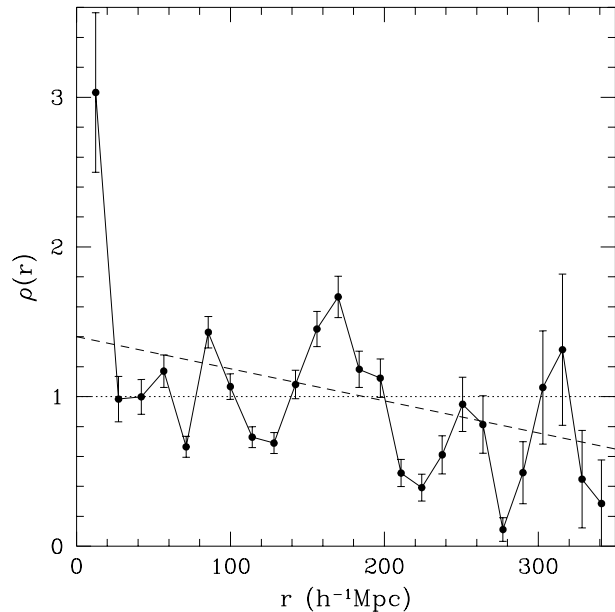
Figure 2. The maximum likelihood estimate for the radial density function. The solution has been normalised to unity in the observed distance range as indicated by the dotted line. Large fluctuations of order ~ 50 per cent are present on $\sim 50 h^{-1}$Mpc scales. Also, the dashed line shows a simple straight line minimum χ^2 fit to the data points. This confirms the visual impression that the radial density is falling with distance.

a faint end upturn down to $M_{b_J} \sim -15$. The results of the likelihood ratio test described in Section 3.1 are also given in Table 1. It is seen that neither of these Schechter functions provide good formal fits to the SWML function, with the convolved Schechter function being marginally better. However, both agree well with the general SWML shape on a qualitative level.

4.2   The Radial Density Shape

The maximum likelihood estimate of the radial density function has been calculated using the method outlined in Section 3.2 and is shown in Fig. 2. The error bars on $\rho(r)$ were also calculated using the techniques described in Section 3.2. The non-parametric stepwise solution converged to 5 *s.f.* after ~ 20 iterations. This solution has been normalised to unity over the plotted distance range.

The observational incompleteness previously described is not explicitly corrected for in this method. One can again weight the p_i's implicit in equation 14 by the appropriate completeness rate to account for this effect. In practice, this correction makes only a small difference to the estimated $\rho(r)$.

Fig. 2 shows that fluctuations in the observed radial density function are of order ~ 40-60 per cent and occur on $\sim 50 h^{-1}$Mpc scales. As we will see the radial distances of the 'peak and trough' fluctuations agree well with the observed number-distance histogram. The observed large local overdensity for $r < 20 h^{-1}$Mpc probably causes the slight faint end excess seen in the VMAX estimate of the luminosity function. Also, it is interesting to see that a straight line
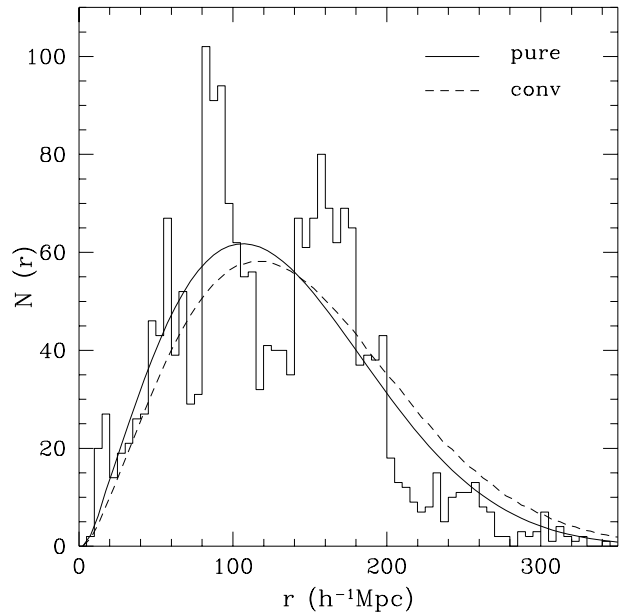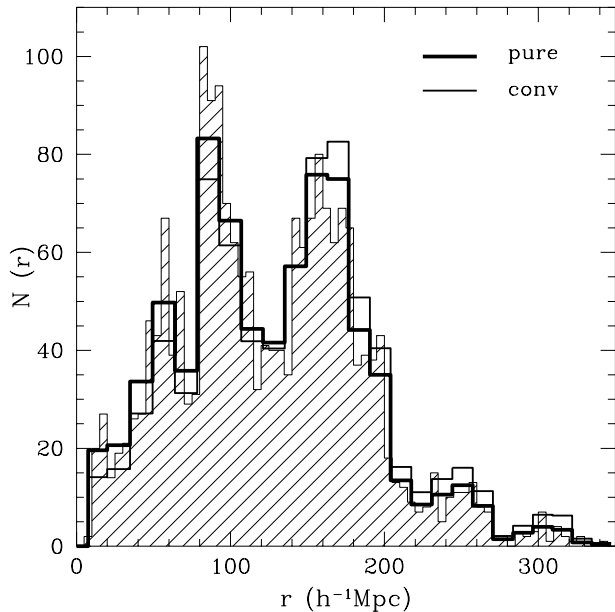

Figure 3. The observed galaxy number-distance histogram, $N(r)$, from the Durham/UKST survey using the magnitude limits described in Section 4. The smooth curves show the expected distribution for a homogeneous sample with this survey's magnitude limits and completeness rates using the maximum likelihood pure Schechter function (solid curve) and convolved Schechter function (dashed curve) of Section 4.1.

minimum χ^2 fit to the radial density function (dashed line) is significantly different from the expected flat slope (dotted line). (This difference remains significant even if we remove the first point from the fit.) Specifically, the $< 200 h^{-1}$Mpc region is ~ 20 per cent overdense and the $> 200 h^{-1}$Mpc region ~ 20 per cent underdense, the error being ~ 4 per cent on each measurement. This is discussed further in Section 5.

Fig. 3 compares the observed galaxy number-distance histogram with two homogeneous models. The magnitude limits and completeness rates from the previous section are used for models and data alike. The two models are the STY maximum likelihood solutions from Table 1 for a pure (unconvolved) Schechter function and a convolved Schechter function. They have been normalised to match the total galaxy number in the sample. These homogeneous models do not provide a detailed fit to the data because of the effects of strong galaxy clustering on scales $> 20 h^{-1}$Mpc. It can be also seen that both models overpredict the numbers of galaxies at $r > 200 h^{-1}$Mpc, with the convolved Schechter function model being slightly worse in this respect.

Comparison of the observed $N(r)$ from Fig. 3 with the radial density function from Fig. 2 shows that the 'peak and trough' fluctuations in $\rho(r)$ agree well with the 'spikes' in $N(r)$. As a consistency test, in Fig. 4 we plot the product of the two homogeneous $N(r)$ models with the observed $\rho(r)$ and compare with the observed $N(r)$. The agreement is impressive, implying that the initial assumption of the luminosity function having a universal form (allowing a separation of variables, see Section 3.1) is justified.

Figure 4. The observed galaxy number-distance histogram, $N(r)$, from the Durham/UKST survey (shaded histogram, see Fig 3). The two bold histograms are the product of the Durham/UKST radial density function (see Fig. 2) and the two number-distance model curves (see Fig 3).
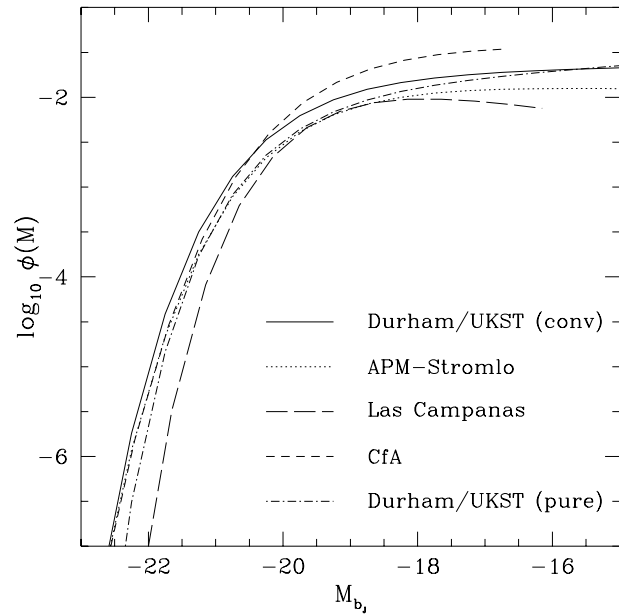
4.3   The Normalisation

The results of the iterative estimator of equations 18 and 19 for $\bar{n}$ are given in Table 1, with $\sim$5 iterations needed for 5 $s.f.$ convergence. The value of ϕ^* is estimated from numerical evaluation of the integral in equation 17. Use of a simple $w = 1$ estimate for $\bar{n}$ (instead of equation 19) makes a $\sim$5 per cent difference to $\bar{n}$. The formal error from equation 21 (using the weighting in equation 19) gives a 7 per cent error in $\bar{n}$. This can be compared with a 10 per cent error for $w = 1$. However, the dominant error comes from the uncertainty in the selection function (due to the uncertainty in the Schechter parameters M^* and α) and is $\sim$15 per cent. This gives a total error in the normalisation of $\sim$17 per cent. Also, for this analysis we choose $M_{low} = -15$ and as previously mentioned in Section 3.3 varying this parameter only causes a small ($\sim$ few per cent) change in ϕ^*.

Obviously for estimates of $\bar{n}$ and ϕ^* the effects of observational incompleteness must be corrected. Therefore, in this analysis the sum in the numerator of equation 17 is weighted by the appropriate completeness rate of the UKST field and apparent magnitude interval of the galaxy in question.

One can comment on the $\sim$40 per cent change in ϕ^* observed with the two different parametric forms. This is caused by a combination of the different relative luminosity function shapes (and the corresponding integrals over them in equations 16, 17 and 18) and the different Schechter function parameters (particularly α). This is discussed further in Section 5.

5   DISCUSSION

Figure 5. Comparison of the normalised Durham/UKST luminosity function with those estimated from recent galaxy redshift surveys. All the magnitudes have been transformed to the blue b_J system. This entails shifting the Las Campanas Gunn-r magnitudes by the average galaxy colour, $\langle b_J - r \rangle_0 = +1.1$ (Tucker 1994; Lin et al. 1996), while the CfA Zwicky magnitudes are shifted by $b_J - M_Z = -0.45$ (Shanks et al. 1984). All of the luminosity functions plotted here are corrected for magnitude errors by convolution of a Gaussian error function with a Schechter function. For reference, we also plot the pure (unconvolved) Durham/UKST Schechter function.

5.1   Comparison with Luminosity Functions from Other Galaxy Redshift Surveys

Table 2 shows a comparison between the parameters of some recently completed galaxy redshift surveys (Loveday et al. 1992; Marzke et al. 1994; Lin et al. 1996) and the Durham/UKST survey. Note that the comparisons given here are for *convolved* Schechter functions because they are the preferred fits as quoted in the literature. However, as was seen in Section 4.1, while the convolved Schechter function did provide a slightly better fit to the SWML luminosity function, the significance was marginal given the extra complexity added to the analysis. As was mentioned in Section 4.2 the pure (unconvolved) Schechter function provides a more realistic fit to the observed number-distance histogram. These normalised luminosity functions are plotted in Fig. 5 where magnitudes have been transformed to the blue b_J system, albeit with only a naive magnitude offset. The Las Campanas galaxies are offset by the average galaxy colour, namely $\langle b_J - r \rangle_0 = +1.1$ (Tucker 1994; Lin et al. 1996). The CfA galaxies are offset by $b_J - M_Z = -0.45$, which comes from the comparison of galaxy number-magnitude count data in Shanks et al. (1984).

Looking at Table 2 shows that the Las Campanas and CfA surveys contain considerably more galaxies than the Durham/UKST or APM-Stromlo surveys. However, in spite of this, all of these surveys sample similar sized volumes (within an order of magnitude) due to the different observ-

Table 2. Comparison of some recent galaxy redshift survey parameters and their corresponding maximum likelihood (convolved) Schechter luminosity functions. While the original passband of the survey is quoted in the left-hand column, the M^*'s in the right-hand column have been transformed to the b_J passband so that a direct comparison can be made ($\langle b_J - r \rangle_0 = +1.1$ and $b_J - M_Z = -0.45$, Tucker 1994; Lin et al. 1996; Shanks et al. 1984).

Survey	Passband	N_{gal}	Volume ($h^{-3}\mathrm{Mpc}^{-3}$)	α	$M_{b_J}^*$	ϕ^* ($h^3\mathrm{Mpc}^{-3}$)
Durham/UKST	b_J	~2100	4×10^6	-1.04 ± 0.08	-19.68 ± 0.08	$(1.7 \pm 0.3) \times 10^{-2}$
APM-Stromlo	b_J	~1800	1×10^7	-0.97 ± 0.15	-19.50 ± 0.13	$(1.4 \pm 0.2) \times 10^{-2}$
Las Campanas	Gunn-r	~19000	1×10^7	-0.70 ± 0.05	-19.19 ± 0.02	$(1.9 \pm 0.1) \times 10^{-2}$
CfA	Zwicky	~9000	1×10^6	-1.0 ± 0.2	-19.25 ± 0.3	$(4.0 \pm 1.0) \times 10^{-2}$

ing strategies used. The accuracy of the quoted ϕ^*'s reflects both the number of galaxies and, more importantly, the total volume surveyed.

Comparing the results in Table 2 and Fig. 5 shows that the general features of these luminosity functions agree well down to $M_{b_J} \sim -17$. Namely, that the characteristic absolute magnitude at the 'knee' is $M_{b_J}^* \simeq -19.4$, the faint end slope is flat, $\alpha \simeq -1.0$, and the overall normalisations agree well (apart from the CfA one which may be biased high by local inhomogeneities). However, fainter than $M_{b_J} \sim -17$ one does find some discrepancies in the values of the faint end slopes. The Durham/UKST and APM-Stromlo surveys agree well and retain a reasonably flat slope. Marzke et al. (1994) claim that the CfA survey has a significant excess of galaxies in this region, $\alpha \simeq -1.3$. Lin et al. (1996) measure a declining faint end slope, $\alpha \simeq -0.7$, from the Las Campanas survey.

We can comment on the results from these other surveys. Firstly, the CfA excess comes mainly from a very local region ($r < 25h^{-1}\mathrm{Mpc}$), which is probably not a representative sample of the Universe. Therefore, while an excess might exist, its significance could be in doubt. Secondly, not only is the Las Campanas survey selected in a different passband (which would cause different relative fractions of galaxy types to be observed), but also this survey is biased against observing low surface brightness galaxies (because of observational selection effects). Therefore, if there is any correlation between low surface brightness and intrinsically faint absolute magnitudes then one can explain their deficit. We also comment on the preliminary luminosity function results from the ESO Slice Project (ESP; Vettolani et al. 1996). They measure a normalisation approximately twice that of the above surveys and a rising faint end slope, $\alpha \simeq -1.2$, for galaxies fainter than $M_{b_J} \sim -17$. At present the significance of their faint end excess is unknown and so we cannot comment on that result. However, given that this survey is complete to a fainter magnitude limit than those discussed here, $b_J \simeq 19.5$, one might expect a higher normalisation because of the steep slope of the observed galaxy number-magnitude counts in this range (e.g. Metcalfe et al. 1995a).

We also note that the form of the Durham/UKST and APM-Stromlo luminosity functions are in good agreement with the combined colour-dependent galaxy luminosity function estimates of Shanks (1990) and Metcalfe et al. (1997). Thus, the increasing slope of the luminosity function of blue, late-type galaxies cancels with the decreasing luminosity function slope of the redder galaxies, leaving an overall lumi-
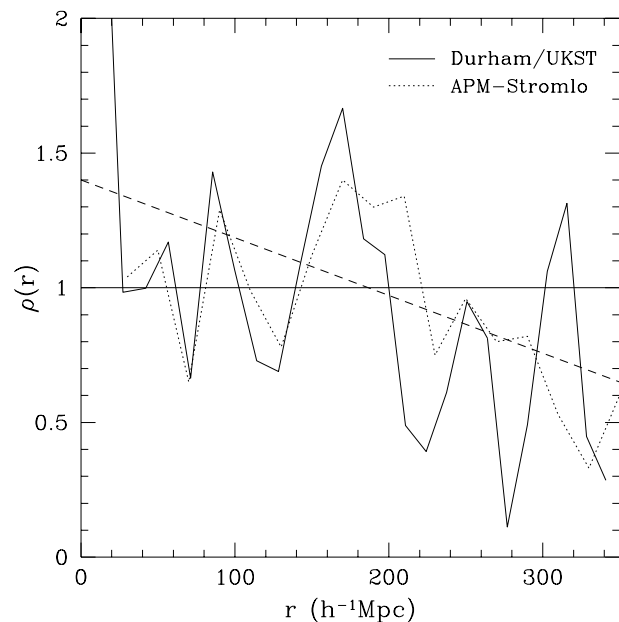
Figure 6. Comparison of the radial density functions, $\rho(r)$, estimated from the Durham/UKST and the APM-Stromlo surveys. These two surveys map a similar overlapping Southern region of space, with the Durham/UKST survey sampling a ~1500 sq. deg. area and the APM-Stromlo survey a ~4300 sq. deg. area. These two solutions have been normalised to unity within each survey. The dashed line shows the minimum χ^2 straight line fit to the Durham/UKST data from Fig. 2.

nosity function which has a flat faint end, which is observed here.

Finally, it is possible to be too pessimistic about the statistical robustness of luminosity function estimates from local magnitude limited surveys (e.g. Driver & Phillipps 1996). We emphasise again that the Durham/UKST luminosity function presented here agrees very well with that of the APM-Stromlo survey, while the observed differences in the other surveys could be caused by slight systematic problems.

5.2   The Radial Density Distribution

Fig. 6 gives a comparison of the radial density functions, $\rho(r)$, for the Durham/UKST and APM-Stromlo surveys. These surveys overlap each other in a Southern region of the sky but map the space slightly differently. The

Durham/UKST survey maps a 'wedge' ($\sim 20° \times 75°$) with 1 in 3 sparse sampling, while the APM-Stromlo survey maps a thicker 'wedge' ($\sim 55° \times 80°$) with 1 in 20 sparse sampling. These two solutions have been normalised to unity within each survey. It can be seen that there is good agreement between the two observed $\rho(r)$'s despite the fact that they do sample slightly different regions of space. In particular, the 'peak and trough' fluctuations are observed in roughly the same places for both surveys. Also, the falling radial density seen in the Durham/UKST survey again appears in the APM-Stromlo survey.

It has previously been suggested that a very large local void, $> 100 h^{-1} \mathrm{Mpc}$ in extent, could explain the low normalisation and steep slope seen in the bright galaxy number-magnitude counts ($b_J < 17$), without the need for evolution (e.g. Shanks 1990). The observed trend in $\rho(r)$ lends support to the idea that large-scale structure *can* affect the counts over a wide magnitude range. However, it should be noted that the decreasing trend in $\rho(r)$ seen in Fig. 6 extends over the whole range of these surveys, out to $z \simeq 0.1$. Since the counts beyond $b_J = 17$ rise to have a $2\times$ higher ϕ^* than at brighter magnitudes this means that $\rho(r)$ will have to rise sharply just beyond the $z \simeq 0.1$ range of the present survey if a large scale structure explanation of the steep galaxy counts is to be possible.

The alternative possibility that the steep counts slope is caused by galaxy luminosity evolution is constrained by the fact that, at $b_J < 21$, the galaxy M^* seems unevolved, which confines any evolutionary explanation to affecting only the intrinsically faint galaxies (Broadhurst, Ellis & Shanks 1988). The observed *decrease* of $\rho(r)$ with distance means that any such evolutionary increase in the numbers of faint galaxies has to be even larger in the range $0 < z < 0.1$ than previously expected to explain the increase in galaxy counts at $17 < b_J < 19$.

We have also considered the possibility that the decreasing radial density $\rho(r)$ could be caused by the effect of cosmology on the volume element. As noted by Weinberg (1972), the effect of q_0 on the volume element with redshift is first order, $dV \propto (1 - \frac{3}{2} q_0 z) dz$; thus even at $z = 0.1$ there is a 15% change in volume for a unit change in q_0. However, the $\rho(r)$ displayed in Fig. 6 was calculated using $q_0 = 0.5$. Assuming a lower value of q_0 such as $q_0 = 0.05$ or $q_0 = -0.5$ would therefore increase the volume element at high redshift and decrease the density at high redshift still further, acting in the opposite manner to that required to reduce the redshift dependence of $\rho(r)$. Thus only a significantly higher value of q_0 than $q_0 = 0.5$ would produce a more homogeneous result and we regard this as less likely than the alternative large-scale structure or evolutionary explanations.

5.3 Comparison with the Cluster Galaxy Luminosity Function

All of the galaxy luminosity functions mentioned so far have been estimated from the field. We can qualitatively compare our results (and those from other redshift surveys) with estimates of the galaxy luminosity function from clusters.

A faint end excess in the cluster galaxy luminosity function ($\alpha \simeq -1.4$) has been known to exist in the Coma and Virgo clusters for quite some time (e.g. Abell 1977; Metcalfe
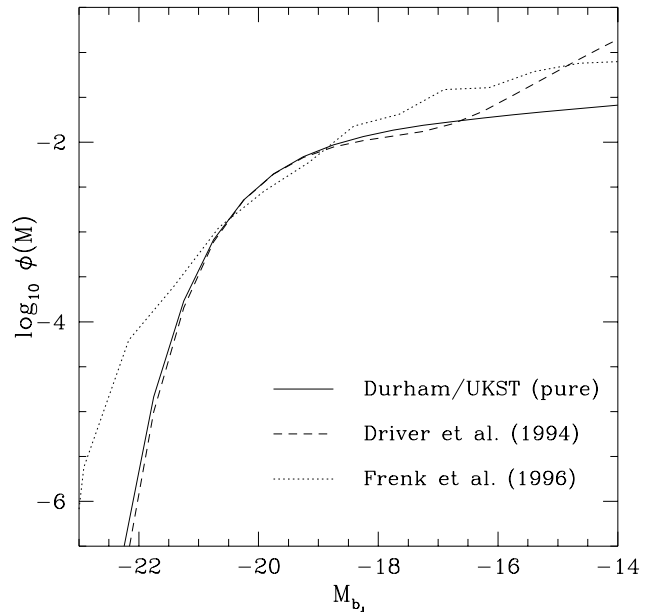
Figure 7. Comparison of the normalised Durham/UKST pure Schechter luminosity function with the cluster galaxy luminosity function model of Driver et al. (1994) and the galaxy formation model of Frenk et al. (1996). The model of Driver et al. (1994) has been made to agree with the Durham/UKST results at M^* and ϕ^*. For the Frenk et al. (1996) results the normalisations are fixed by the model.

1983; Binggeli, Sandage & Tammann 1985). Recent work has confirmed these initial results and extended the observations to other clusters (e.g. Biviano et al. 1995; Kashikawa et al. 1995). Driver et al. (1994) and Wilson et al. (1996) have also studied clusters at higher redshifts ($z \sim 0.2$) and observe a similar steeply rising upturn at the faint end. The overall conclusion is that a single Schechter function cannot provide an adequate fit to such luminosity functions. In all of this recent work the cluster galaxy luminosity function appears better fit by a 2-component Schechter-like function with a flat bright slope ($\alpha \sim -1$) and a steep upturn ($\alpha \sim -2$) for galaxies fainter than $M^* + 2$.

In Fig. 7 we compare the STY results for the pure Schechter function of Section 4.1 with the model proposed by Driver et al. (1994). This model approximates the general cluster luminosity function discussed above and has been translated in the M_{b_J} and ϕ direction to match the Durham/UKST results in M^* and ϕ^*. As might be expected (given the above discussion) this form does not give a particularly good representation of the Durham/UKST results at the faint end of the luminosity function (similarly for the APM-Stromlo and Las Campanas luminosity functions). On the other hand, it is tempting to say that the results from the CfA and ESP surveys match this form of luminosity function. Overall, the errors in the faint ends of both the cluster and field luminosity functions are probably large enough such that no significant inconsistencies currently exist between the two functions.

5.4 Comparison with Current Models of Galaxy Formation

One can also qualitatively compare our results with those from current models of galaxy formation and evolution. These models approach the galaxy formation problem by combining the results of N-body/hydrodynamic simulations with semianalytic modelling techniques (e.g. Cole et al. 1994).

In order to successfully model galaxy formation one needs to include many distinct physical processes, as well as an underlying cosmological structure formation model. These processes include the evolution of dark matter halos, the dynamics of gas cooling, star formation and feedback, the evolution of the stellar populations that form and how galaxies merge and interact. One approximates these processes by a set of simple rules which then form the basis of a semianalytic model of galaxy formation (e.g. Kauffmann et al. 1993; Lacey et al. 1993; Cole et al. 1994). The models are then used to predict and compare with the observable properties of the galaxy distribution, such as the faint galaxy number-magnitude counts, galaxy colours and the galaxy luminosity function.

Fig. 7 also compares the pure Schechter function STY results from Section 4.1 with the semianalytic galaxy formation model of Frenk et al. (1996). The details of this fiducial model are described in Cole et al. (1994) with recent updates from Frenk et al. (1996) and Baugh et al. (1996). One can see that, given the complex modelling involved, this is a reasonable approximation to the luminosity function around M^*. Note that the excess of very bright galaxies has been previously documented (e.g. Frenk et al. 1996). Also, the model predicts a steep faint end slope to the luminosity function. Although this is more in line with the faint end excess seen in the CfA and ESP surveys, we have argued that these are less reliable estimates of the *local* galaxy luminosity function, which we believe is better represented by the results from the Durham/UKST, APM-Stromlo and Las Campanas surveys.

6 CONCLUSIONS

We have estimated the galaxy luminosity function from the Durham/UKST Galaxy Redshift Survey. We use standard maximum likelihood techniques that are unbiased by density inhomogeneities and an optimal weighting function for estimating the normalisation. For a standard Schechter function we find $M_{b_J}^* = -19.72 \pm 0.09$, $\alpha = -1.14 \pm 0.08$ and $\phi^* = (1.2 \pm 0.2) \times 10^{-2} h^3 \mathrm{Mpc}^{-3}$.

Correcting for the observed scatter in our measured magnitudes causes a flatter faint end slope to be measured ($\alpha = -1.04 \pm 0.08$), although this does not significantly improve the quality of the fit. A combination of the change in the shape of the functional form and the flatter α then causes a higher normalisation to be estimated, $\phi^* = (1.7 \pm 0.3) \times 10^{-2} h^3 \mathrm{Mpc}^{-3}$.

Comparison with other recent estimates of the galaxy luminosity function from redshift surveys gives good agreement for absolute magnitudes brighter than $M_{b_J} \sim -17$. Fainter than this absolute magnitude there are some discrepancies in the measured value of α, ranging from -0.7 to -1.3. The Durham/UKST survey lies approximately in the middle of this range and is in very good agreement with the results from the APM-Stromlo survey.

The radial density function has been estimated from the Durham/UKST survey using a maximum likelihood technique. This shows evidence for a falling galaxy density with radial distance, suggesting that large-scale structure may affect the form of the galaxy number magnitude counts in the range $14 < b_J < 19$.

We have shown that the result of forming the product of the radial density function with homogeneous models which assume the above luminosity functions gives good agreement with the observed number-distance histogram. This result is consistent with the initial assumption that the galaxy luminosity function has a universal form.

Our luminosity function results for the field agree with those derived from galaxies in clusters, except at the faint end where the cluster luminosity function appears to be steeper.

Finally, we have compared our results with the predictions of current models of semi-analytic galaxy formation and evolution. These also disagree with our luminosity function at the faint end, where the galaxy formation models predict a significantly steeper luminosity function slope.

REFERENCES

Abell G.O., 1977, ApJ, 213, 327
Baugh C.M. et al., 1996, preprint
Binggeli B., Sandage A., Tammann G.A., 1985, AJ, 90, 1681
Biviano A., Durret F., Gerbal D., Le Fevre O., Lobo C., Mazure A., Slezak E., 1995, A&A, 297, 610
Broadbent A., 1994, private commumication
Broadhurst T., Ellis R.S., Shanks T., 1988, MNRAS, 235, 827
Cole S., Aragõn-Salamanca A., Frenk C.S., Navarro J.F., Zepf S.E., 1994, MNRAS, 271, 781
Collins C.A., Heydon-Dumbleton N.H., MacGillivray H.T., 1988, MNRAS, 236, 7P
Collins C.A., Nichol R.C., Lumsden S.L., 1992, MNRAS, 254, 295
da Costa L.N., Pellegrini P.S., Davis M., Meiksin A., Sargent W.L., Tonry J.L., 1991, ApJS, 75, 935
Davis M., Huchra J., 1982, ApJ, 254, 437
Driver S.P., Phillipps S., Davies J.I., Morgan I., Disney M.J., 1994, MNRAS, 268, 393
Driver S.P., Phillipps S., 1996, preprint
Efstathiou G., in Lawrence A., ed., 3rd *IRAS*, Conference, London, Comets to Cosmology. Springer, Berlin, p. 312
Efstathiou G., Ellis R.S., Peterson B.A., 1988, MNRAS, 232, 431
Ellis R.S., Colless M., Broadhurst T., Heyl J., Glazebrook K., 1996, MNRAS, 280, 235
Fairall A.P., Jones A., 1988, Publs. Dept. Astr. Cape Town, 10
Frenk C.S., Baugh C.M., Cole S., 1996, in *IAU* Symposium No. 171, p. 247

Kashikawa N., Shimasaku K., Yagi M., Yasuda N., Doi M., Okamura S., Sekiguchi M., 1995, ApJ, 452, L99

Kauffmann G., White S.D.M., Guiderdoni B., 1993, MNRAS, 264, 201

Lacey C.G., Guiderdoni B., Rocca-Volmerange B., Silk J., 1993, ApJ, 402, 15

Lilly S.J., Tresse L., Hammer F., Crampton D., Le Fevre O., 1995, ApJ, 390, 338

Lin H., Kirchner R.P., Shectman S.A., Landy S.D., Oemler A., Tucker D.L., Schechter P.L., 1996, ApJ, 464, 60

Loveday J., Peterson B.A., Efstathiou G., Maddox S.J., 1992, ApJ, 390, 338

Marzke R.O., Huchra J.P., Geller M.J., 1994, ApJ, 428, 43

Metcalfe N., 1983, PhD thesis, Univ. of Oxford

Metcalfe N., Fong R., Shanks T., Kilkenny D., 1989, MNRAS, 236, 207

Metcalfe N., Shanks T., Fong R., Roche N., 1995a, MNRAS, 273, 257

Metcalfe N., Fong R., Shanks T., 1995b, MNRAS, 274, 769

Metcalfe N., Ratcliffe A., Fong R., Shanks T., 1997, MNRAS, submitted

Parker Q.A., Watson F.G., 1995, in Maddox S.J., Aragón-Salamanca A., eds., 35th Herstmonceux Conf. Cambridge, Wide Field Spectroscopy and the Distant Universe. World Scientific, Singapore, p33.

Peterson B.A., Ellis R.S., Efstathiou G.P., Shanks T., Bean A.J., Fong R., Zen-Long Z., 1986, MNRAS, 221, 233

Ratcliffe A., 1996, PhD thesis, Univ. of Durham

Ratcliffe A., Shanks T., Broadbent A., Parker Q.A., Watson F.G., Oates A.P., Fong R., Collins C.A., 1996, MNRAS, 281, L47

Sandage A., Tammann G.A., Yahil A., 1979, ApJ, 232, 352

Saunders W., Rowan-Robinson M., Lawrence A., Efstathiou G.P., Kaiser N., Ellis R.S., Frenk C.S., 1990, MNRAS, 242, 318

Schechter P.L., 1976, ApJ, 203, 297

Schmidt M., 1968, ApJ, 151, 393

Shanks T., 1990, in *IAU* Symposium No. 139, p. 269

Shanks T., Stevenson P.R.F., Fong R., MacGillivray H.T., 1984, MNRAS, 206, 767

Tucker D.L., 1994, PhD thesis, Univ. of Yale

Vettolani P. et al., 1996, preprint

Weinberg S., 1972, Gravitation and Cosmology, Wiley, NY

Wilson G., Smail I., Frenk C.S., Ellis R.S., Couch W.J., 1996, MNRAS, in press